communications biology

A Nature Portfolio journal

Article

https://doi.org/10.1038/s42003-025-09049-w

Cannabinoids shift the basal ganglia microRNA m^{6}A methylation profile towards an anti-inflammatory phenotype in SIV-infected rhesus macaques

Chioma M. Okeoma [1,2] ✉, Lakmini S. Premadasa[3], Chen S. Tan[4], Ionita C. Ghiran [5] ✉ & Mahesh Mohan [3] ✉

Epitranscriptomic modifications [N6-methyladenosine (m^{6}A)] regulate various diseases, including cancer and inflammation. Despite their functional relevance in neural development and differentiation, the role of m^{6}A modifications in HIV neuropathogenesis is unknown. Using anti-N6-methyladenosine (m^{6}A) antibody-immunoprecipitation and microarray profiling, we identified m^{6}A modifications in miRNAs in basal ganglia (BG) of uninfected (VEH) and SIV-infected Rhesus macaques (RMs) on combination anti-retroviral therapy (ART) and either VEH-treated (VEH/SIV/ART) or THC:CBD-treated (THC:CBD/SIV/ART). HIV/SIV infection promoted an overall hypomethylated miRNA m^{6}A profile. While THC:CBD did not significantly impact the overall hypomethylated m^{6}A profile, specific miRNAs predicted to target proinflammatory genes showed marked m^{6}A hypomethylation compared to VEH-treated RMs. Additionally, specific BG m^{6}A-modified miRNAs were detected in BG-derived extracellular vesicles. Mechanistically, the DRACH motif in the miR-194-5p seed region was significantly m^{6}A hypomethylated in THC:CBD/SIV/ART RMs. Unlike wild-type, in-vitro transfected m^{6}A-modified miR-194-5p mimics failed to downregulate STAT1 protein expression. Further, compared to VEH/SIV/ART RMs, THC:CBD significantly reduced m^{6}A methylation of 44 miRNAs directly involved in regulating CNS network genes. Our findings indicate that m^{6}A epi-transcriptomic marks in the seed nucleotides can impair miRNA function and that cannabinoids may preserve it by reducing m^{6}A methylation levels, thus providing a mechanistic explanation underlying their anti-neuroinflammatory effects in HIV/SIV infection.

Despite successful control of HIV with combined antiretroviral therapy (ART)[1–3], up to 50% of persons living with HIV (PLWH) still suffer from HIV-Associated Neurocognitive Disorders (HAND)[4,5]. A major factor driving HAND is incomplete viral suppression in the CNS and the consequent activation of resident microglia, leading to neuroinflammation and neuronal damage.

In addition, drug abuse is a major comorbidity, where ~40% of PLWH use cocaine and cannabis[6–9], resulting in increased virus-induced pathology[10–15], though cannabis use could afford varying degrees of protection from immune activation/inflammation[7]. While collecting longitudinal blood and matched brain samples from PLWH and healthy subjects is extremely challenging, the availability of the SIV-infected rhesus macaque (RM) model supports the investigation of the effects of phytocannabinoids and other drugs of abuse on HIV/SIV neurological disease progression and has the potential to shed light on the underlying molecular mechanisms. Our previous studies showed that twice daily administration of low-dose delta-9-tetrahydrocannabinol (THC) significantly reduced expression of type I-interferon (IFN)-induced genes including inflammation-associated

[1]Department of Pathology, Microbiology & Immunology, New York Medical College, Valhalla, NY, USA. [2]Lovelace Biomedical Institute, Albuquerque, NM, USA. [3]Southwest National Primate Research Center, Texas Biomedical Research Institute, San Antonio, TX, USA. [4]Division of Infectious Diseases, Department of Internal Medicine, Carver College of Medicine, University of Iowa, Iowa City, IA, USA. [5]Department of Anesthesia, Critical Care and Pain Medicine, Beth Israel Deaconess Medical Center, Harvard Medical School, Boston, MA, USA. ✉e-mail: cokeoma@nymc.edu; ighiran@bidmc.harvard.edu; mmohan@txbiomed.org

miRNAs, miR-155 and miR-142-3p, in the basal ganglia (BG) of ART-naïve SIV-infected RMs[16,17]. The effect of THC on BG was also present in BG-derived extracellular vesicles (EVs). Transcriptomic analyses of miRNAs associated with EVs isolated from these BG tissues revealed that both SIV infection and THC administration induced distinct but significant changes in BG EV-associated miRNAs, which were predicted to regulate pathways related to inflammation/immune regulation, TLR signaling, neurotrophin TRK receptor signaling, and cell death/response[18]. Long-term administration of low-dose THC to SIV-infected RMs led to significant upregulation of 37 miRNAs in BG-EVs. Out of the 37 miRNAs, 11 were significantly downregulated in EVs from SIV-infected RMs that received an equal volume of vehicle but not THC.

Recent studies have identified over 170 RNA modifications, among which, m^{6}A (N6-methyladenosine) is the most abundant modification in mammalian RNA, occurring in ~50% of the total methylated ribonucleotides[19]. RNA m^{6}A modifications regulate a wide variety of processes such as metabolism, splicing, translation, and degradation of RNA as well as in disease pathogenesis. M^{6}A modifications have been described not only in mRNA but also recently in miRNAs, a class of small noncoding regulatory RNAs. miRNAs play key roles in regulating protein translation and have been implicated in various neurological disorders, including cognitive impairment. While others and we have published the role of miRNAs in the regulation of gene expression in the brain, there is a significant knowledge gap regarding the role of post transcriptional changes, in particular, miRNA m^{6}A modification and its implications in HIV/SIV neuropathogenesis. Accordingly, the present study investigated the relationship between HIV/SIV infection of BG, miRNA m^{6}A alterations, and the potential impact of concurrent phytocannabinoid use on miRNA m^{6}A modifications and its potential implications for HAND pathogenesis.

Here, we present data supporting shifts in the small RNA landscape in the BG in response to HIV/SIV infection and ART treatment and the impact of concurrent THC:CBD administration. In addition to changes in the expression levels of several miRNA species involved in cognition and neuroinflammation, we also for the first time detected significant alterations in the m^{6}A methylation levels of key miRNA species, suggesting an added, more refined level of protein expression control. By exploring the interplay involving HIV/SIV infection, miRNA m^{6}A alterations in BG, and phytocannabinoid administration, this study aims to offer a comprehensive overview and understanding of the role of m^{6}A modifications on miRNA function that may provide valuable mechanistic insights into the development of HAND and pave the way for novel therapeutic strategies to mitigate CNS disease in PLWH.

Results

Quantification of m^{6}A profiles of BG miRNAs identified mechanistically relevant species involved in the anti-inflammatory effect of THC:CBD administration

Altered m^{6}A-modified RNA expression levels in the brain were linked to dysregulation of key genes involved in immune cell activation, cytokine production, and blood-brain barrier integrity, which could modulate the activation of microglia and astrocytes, thereby initiating and exacerbating neuroinflammatory processes[20,21]. Most of the published research regarding the role of m^{6}A changes in neuroinflammation has centered on mRNA and lncRNA and not miRNA molecules (reviewed in ref. 22). Hence, we focused exclusively on miRNAs in the present study.

All seven SIV-infected RMs, receiving either VEH (n = 4) or THC:CBD (n = 3), had substantial plasma viral loads ranging from 1.93 to 16.8 × 106 copies/mL during acute infection [12-20 days post SIV infection (DPI)] (Table 1). However, ART initiation at 30 DPI effectively suppressed viral replication, as viral RNA was undetectable in both plasma and BG at necropsy (180 DPI).

We investigated how SIV infection and/or THC: CBD altered the landscape of m^{6}A changes in miRNAs isolated from BG of RMs that were either i) uninfected (Control), ii) SIV-infected, treated with ART, and administered either vehicle (VEH) alone (VEH/SIV/ART), or iii) SIV-infected, treated with ART, and administered THC: CBD (THC-CBD/SIV/ART). The m^{6}A analyses were performed by microarray hybridization profiling following pull-down of m^{6}A-modified miRNAs using an m^{6}A-specific antibody (Synaptic Systems). BG tissues from all three groups were analyzed for miRNA m^{6}A modifications. After quality control and filtering, we used a p-value (unpaired t-test) <= 1.0 and fold-change >= 0.0 to identify a total of 1805 miRNAs that were m^{6}A modified in all experimental groups irrespective of statistical significance (Supplementary Table 1 and Supplementary Data 1). We compared each treatment group to the uninfected control group and found that SIV infection under suppressive ART induced a significantly broader m^{6}A hypomethylation of BG miRNAs (Supplementary Table 2) compared to hypermethylation. Out of the total 1805 miRNAs in the VEH/SIV/ART group with m^{6}A modifications, 1281 (71%) were mature miRNAs, while 524 (29%) were passenger strand (PS) miRNAs (generated from the opposite (3') strand) (Fig. 1a). Over 95% of the mature and PS miRNAs were m^{6}A hypomethylated in VEH/SIV/ART (Fig. 1b) and in THC:CBD/SIV/ART (Fig. 1c) RMs compared to uninfected controls (Fig. 1b, c). In contrast, only 6% and 5% of mature and PS miRNAs, respectively, were hypomethylated when comparing VEH/SIV/ART to THC:CBD/SIV/ART (Fig. 1d) RMs. Raw intensities of immunoprecipitated m^{6}A- and unmodified-miRNA species, respectively, were normalized with the average of log2-scaled spike-in RNA intensities. We found an overall inverse relationship between m^{6}A methylation and expression abundance of the miRNA species in VEH/SIV/ART (Fig. 1e) and THC:CBD/SIV/ART (Fig. 1f) RMs when compared to controls and that of VEH/SIV/ART when compared to THC:CBD/SIV/ART (Fig. 1g) RMs. Our data presented above show that while unsupervised clustering of the differentially expressed miRNA species isolated from BG fails to separate the control from the THC:CBD-treated group, analyses of the differentially m^{6}A-modified miRNA clearly identify changes in the miRNA profile promoted by THC:CBD administration, underscoring the need for functional quantification of the RNA levels in addition to the canonical up and down quantifications.

SIV infection increased the overall m^{6}A methylation levels in BG-derived miRNAs

Further analyses of the m^{6}A-methylated miRNAs were conducted to identify significantly m^{6}A-modified miRNAs using p-value < 0.05 (unpaired t-test) and fold change>= 1.5. We found that most of the m^{6}A-modified miRNAs were present in mature miRNAs with percentages ranging from 60 to 72% (Fig. 2a–f). While SIV infection induced significant hypomethylated m^{6}A modifications in BG miRNAs in over 1000 miRNA species when compared to control animals, hypermethylation changes were identified in only seven miRNA species (Supplementary Table 2). We next compared methylation levels with miRNA abundance (expression) by calculating the miRNA abundance using mean m^{6}A RNA modification quantity per treatment, mean m^{6}A RNA modification quantity for control, and the difference in mean percentage of m^{6}A RNA modification (% Modified) between the treatment and control groups. The levels of the m^{6}A modification versus abundance are displayed as heatmaps (Fig. 2g–l). The top 5 miRNAs or fewer (depending on the group) were selected, and their m^{6}A and expression levels are presented as heatmaps (Fig. 2m–r).

Pathway analysis of SIV-induced m^{6}A epi-transcriptomic marks in BG miRNAs identified top neuroinflammation network genes

To analyze the biological implications of m^{6}A-enriched miRNAs, we used ingenuity pathway analysis (IPA) to perform enrichment analysis of predicted and validated genes targeted by m^{6}A hypo- or hypermethylated miRNAs (Supplementary Table 1) using criteria determined apriori. We identified neuroinflammation network genes associated with the miRNAs from each group that were hypomethylated (Supplementary Fig. 1 left panels and Fig. 3a) or hypermethylated (Supplementary Fig. 1 right panels and Fig. 3b). The top 35 IPA neuroinflammation network genes associated with m^{6}A hypo- and hypermethylated miRNAs are shown in Supplementary Table 3. In addition to the protein networks altered by the

Table 1 | Animal IDs, SIV inoculum, duration of infection and viral loads in combination anti-retroviral therapy treated chronic SIV-infected rhesus macaques receiving vehicle or Δ^9-THC :CBD combination

Animal ID	SIV Inoculum	Duration of Infection (days)	12 DPI Plasma viral loads (10^6/mL)	Plasma Viral loads at necropsy (10^6/mL)	Basal Ganglia viral loads at necropsy (10^6/mg)	Opportunistic Infections
Chronic SIV-Infected, ART and Vehicle treated						
VSART1	SIVmac251	180	2.50	ND	ND	ND
VSART1	SIVmac251	180	5.43	ND	ND	ND
VSART1	SIVmac251	180	1.93	ND	ND	ND
VSART1	SIVmac251	180	2.23	ND	ND	ND
Chronic SIV-Infected, ART and THC:CBD treated						
TCART1	SIVmac251	180	8.2 *	ND	ND	ND
TCART2	SIVmac251	180	15.8 *	ND	ND	ND
TCART3	SIVmac251	180	16.8 #	ND	ND	ND
Uninfected Controls						
Control 1	NA	NA	NA	NA	NA	NA
Control 2	NA	NA	NA	NA	NA	NA
Control 3	NA	NA	NA	NA	NA	NA
Control 4	NA	NA	NA	NA	NA	NA

ND None detected.
NA Not applicable.
* - 20 DPI viral load.
# - 30 DPI viral load.
DPI Days post SIV Infection.

m^6A-methylated miRNAs, our results also identified several miRNA species that were targeted by the m^6A-modified miRNAs. These data are consistent with previous reports that demonstrated regulation of primary miR-21 by mature miR-122[23–25].

Integration of IPA and GO analyses

Our analyses identified several disease-related functional clusters linked to neuroinflammation network genes associated with m^6A hypo- and hypermethylated miRNAs (Supplementary Table 4). Whereas the top three diseases related to changes in invasion, migration, and proliferation of cells were linked to a hypomethylated m^6A profile (rows 1-4), diseases associated with changes in quantity of cells, organization of cytoskeleton, and neurotransmission were linked to the hypermethylated m^6A profile (rows 1–-3). Integration of IPA and the 35 neuroinflammation genes with the WEB-based Gene SeT Analysis Toolkit (WebGestalt) GO analysis identified several biological processes, cellular components, and molecular functions of the neuroinflammation network genes for each group that stratified into targets of m^6A hypomethylated (Fig. 4a) and hypermethylated (Fig. 4b) miRNAs.

Conjoint Analysis of m^6A methylation and differentially altered miRNA expression

We next determined the functional significance of m^6A methylation of miRNAs by first determining the relative abundance of the m^6A hypo- and hypermethylated miRNA species. After obtaining the abundance of miRNAs with significant m^6A modifications, we found that the majority of significantly m^6A-modified miRNAs were either significantly up- or down-regulated (Supplementary Table 5). We also found a positive correlation between m^6A methylation and miRNA abundance for Hypo_VEH/SIV/ART_vs_Controls (Pearson r = 0.72; p < 1e-10) and Hypo_THC:CBD/SIV/ART_vs_Controls (Pearson r = 0.84; $p < 1e^{-10}$) (Fig. 5a, b), respectively. However, we did not identify any additional correlations among other treatment groups (Supplementary Fig. 2). To examine the functional relationship of m^6A-methylated miRNAs, we used IPA miRNA Target Filter focused on miRNAs related to neurotransmitter networks and nervous system-centered signaling pathways (Fig. 5c–h and Supplementary Data 2). Analysis of protein-protein interactions (PPI) for the IPA identified miRNA targets using STRING: functional protein association networks (https://string-db.org/) led to the identification of several gene clusters and nodes associated with the m^6A methylation status (hypermethylation vs. hypomethylation) and miRNA abundance that may shed light on the potential biological functions of miRNA m^6A methylation (Fig. 5i-n). The potential biological functions of the miRNA targets were further revealed by GO biological processes, molecular functions, cellular components, Kegg/Reactome/Wiki pathways, disease gene associations, and tissue expressions (Supplementary Data 3).

THC: CBD administration significantly reduced the m^6A levels in the seed sequence of HIV/SIV-altered miRNAs demonstrated to regulate neuroinflammation

Relative to the THC: CBD/SIV/ART group, 44 miRNAs showed significant m^6A hypermethylation in the VEH/SIV/ART RMs (Fig. 6a). More importantly, IPA analyses of the genes targeted by the 44 miRNAs that were hypermethylated in the BG of VEH/SIV/ART compared to THC:CBD/SIV/ART RMs identified neuroinflammation gene networks previously shown to drive neuroinflammation and neuropathogenesis of Huntington's, Alzheimer's, and Parkinson's disease (Fig. 6b). Key biological processes regulated by these m^6A hypermethylated miRNAs included the gamma-aminobutyric acid signaling pathway, synaptic transmission, cognition, immune-response regulating signaling pathway, and positive regulation of cytokine production (Fig. 6c). GABA receptor activity, glutamate receptor activity, neurotransmitter receptor activity, gated channel activity, and cytokine receptor activity were the most significant molecular functions enriched for these mRNA targets. Additionally, the targets of the miRNAs associated with KEGG were linked to GABAergic synapse, leishmaniasis, and nicotine addiction. Reactome pathways are linked to the Toll-like receptor 5 cascade, the MyD88 cascade, neurotransmitter receptors, and postsynaptic signal transmission, signaling by interleukins, and cytokine signaling in the immune system. Diseases associated with autistic disorder, asthma reperfusion injury, atherosclerosis, substance withdrawal syndrome, nerve degeneration, cholestasis, myocardial reperfusion injury, urticaria, and hepatic encephalopathy (Supplementary Fig. 3a-c). Further analysis of the 44 m^6A hypermethylated miRNAs revealed an RRACH or DRACH motif in 14 out of the 44 miRNAs (Supplementary Table 6), indicating that

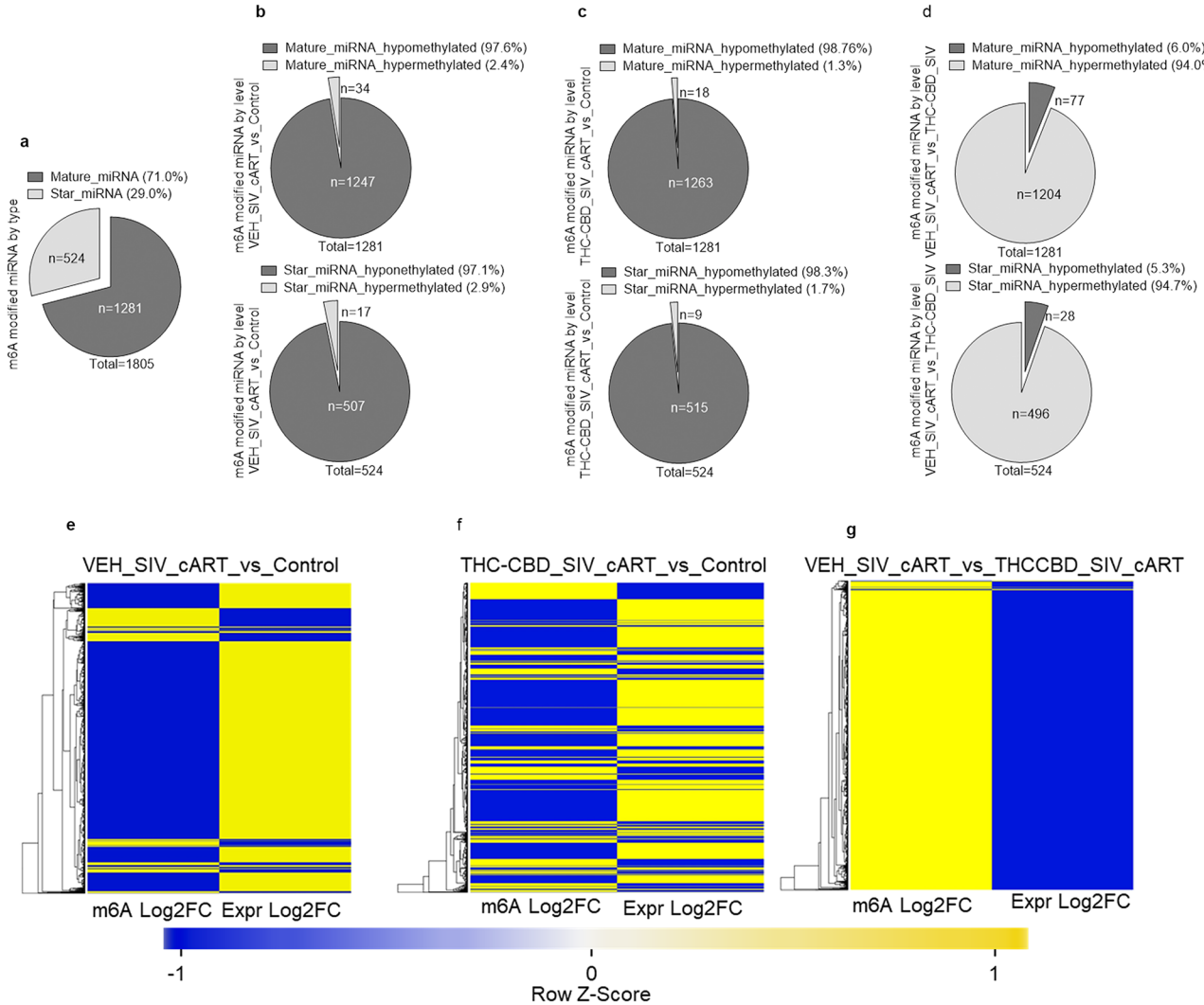

Fig. 1 | Global m^{6}A methylation patterns of basal ganglia miRNAs of rhesus macaques infected with SIV and treated with Vehicle and, ART, or THC:CBD and ART over uninfected controls. a Percent mature and passenger (*) strand miRNAs with m^{6}A methylation marks. **b–d** m^{6}A methylation patterns in each treatment group. **e–g** Heatmap of m^{6}A methylation profile versus miRNA abundance.

the rest of the m^{6}A methylation events took place in non-canonical DRACH motifs[26]. The IPA network linked the targets of the 14 miRNAs with the RRACH or DRACH motif to canonical signaling pathways of NF-kB activation by viruses, neuroinflammation signaling, and transcriptional activity by SMAD heterotrimer, all of which are functionally linked to cognitive impairment[27–29] (Fig. 6d).

M^{6}A marks in the miR-194-5p seed region impaired its potential to post-transcriptionally silence the proinflammatory STAT1 protein in vitro

Since miR-194-5p showed significantly more m^{6}A hypomethylation in the BG of THC:CBD/SIV/ART (-1.6683 log2 Fold change or -3.178 Fold change) than VE/SIV/ART (-0.8617 log2 Fold change or -1.817 fold change) RMs compared to controls and ~1.74-fold ($p = 0.06$) more hypomethylation in BG of THC:CBD/SIV/ART relative to VEH/SIV/ART RMs (Fig. 7b), we hypothesized that this would allow miR-194-5p to more effectively downregulate its highly conserved (Fig. 7a)[30] predicted target gene, STAT1, an interferon-gamma stimulated transcription factor known to activate the expression of interferon-stimulated immune response genes and drive neuroinflammation in PWH and SIV infected RMs[31]. To investigate the impact of m^{6}A epitranscriptomic marks on miR-194-5p-STAT1 interactions, we synthesized locked nucleic acid conjugated FAM-labeled m^{6}A methylated miR-194-5p (in the seed nucleotide region) mimics along with wild-type miR-194-5p and negative control (NC) mimics and transfected SCC-25 oral squamous cell carcinoma cells. We used SCC-25 cells since they expressed high basal STAT1 protein levels (Supplementary Fig. 4a, b). In contrast, the two neuronal cell lines we had access to, namely, HCN2 neuronal and SH-SY5Y neuroblastoma (Supplementary Fig. 4c, d) cells, showed very low to no basal STAT1 protein expression. Using RNAhybrid[32], we found the miR-194-5p-STAT1 duplex to have a minimum free energy of -19.8 kcal/mol (Fig. 7c). As evident in Fig. 7e1 and e2, transfection of SCC-2 cells with 30 nM wild-type miR-194-5p significantly reduced STAT1 protein expression compared to the wells transfected with negative control (Fig. 7d1, d2, and g). Consistent with our hypothesis, adding m^{6}A marks to the DRACH motif in the miR-194-5p seed region (Fig. 7c) significantly diminished its ability to suppress STAT1 protein expression (Fig. 7f1, f2, and g). Accordingly, STAT1 protein expression was significantly higher in cells transfected with m^{6}A-modified miR-194-5p mimics (Fig. 7f1, f2, and g) compared to cells transfected with wild type miR-194-5p mimics (Fig. 7e1, e2, and g) but similar to the wells transfected with NC mimics (Fig. 7d1, d2, and g).

Basal ganglia tissue miRNAs enriched in m^{6}A modification are also present in basal ganglia-derived Extracellular Vesicles (EVs)

We integrated BG tissue miRNA abundance with miRNA counts from our previously published BG-derived EVs (BG EVs) miRNA sequence dataset[18]

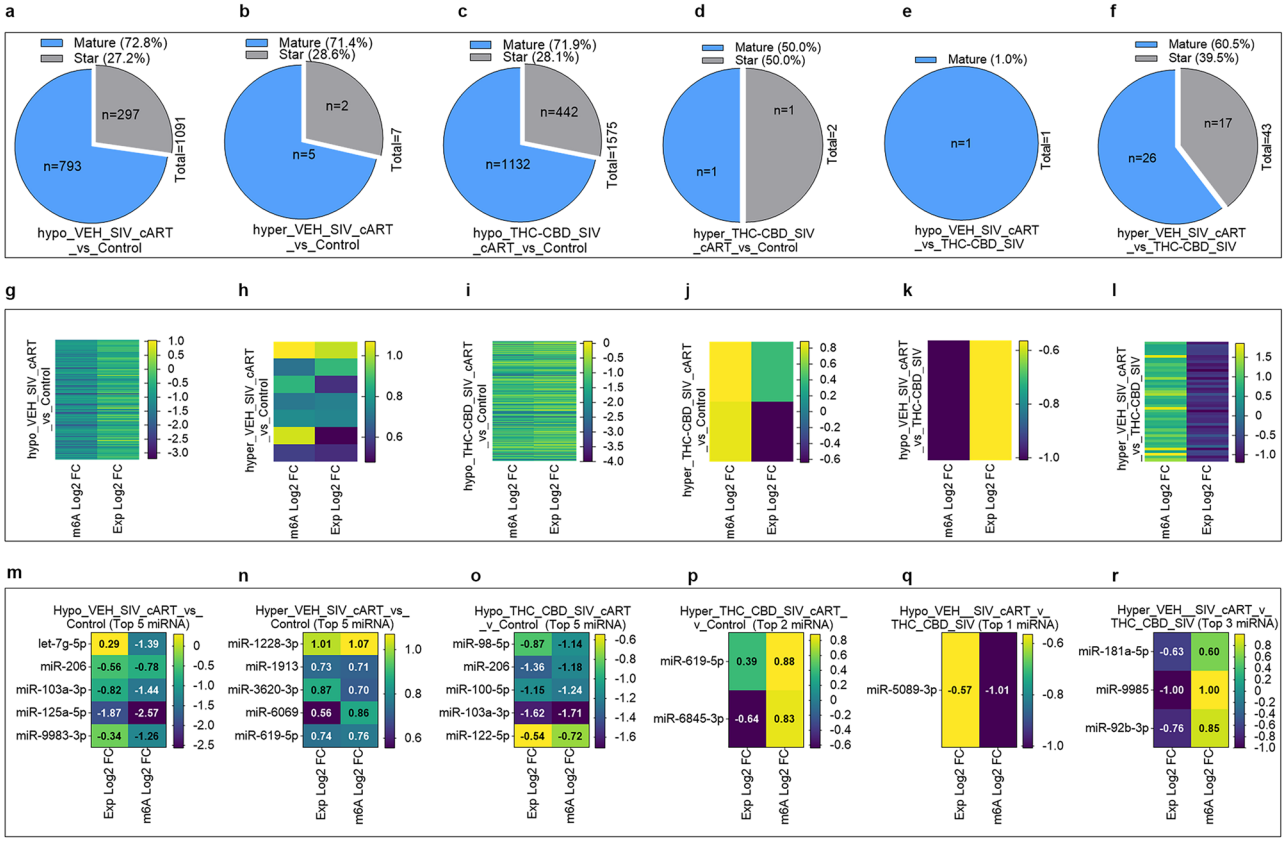

Fig. 2 | The m^{6}A content of rhesus macaque basal ganglia tissues is significantly altered by SIV infection and THC:CBD administration. a–f Pie chart representing the percentage of mature and passenger (*) strand miRNAs with m^{6}A modifications. **g–l** Heatmap illustrating the levels of the m^{6}A methylated miRNAs and their abundance. **m–r** Heatmap of Top 5 miRNAs from (**g–l**).

to identify tissue miRNAs with m^{6}A modifications that were also present in the BG EVs dataset. Of the 527 miRNAs identified in EVs from the BG of SIV-infected RMs, 162 (11.1%) were also present in RM whole BG tissues (Fig. 8a). Although methylation analyses were not conducted on the EV-derived miRNAs, all 162 miRNAs were m^{6}A hypomethylated in the BG tissues, and none were m^{6}A hypermethylated in the EVs, suggesting either a sorting mechanism based on the methylation status of the miRNAs or an active demethylation process performed by m^{6}A erasers, which may be present in EVs (Fig. 8a). The top 5 EV-associated miRNAs belonged to the let-7 family (let-7a-5p, let-7c-5p, let-7b-5p, miR-26a-5p, let-7f-5p) (Fig. 8b) and were different from the top 5 (miR-320b, miR-504-3p, miR-1224-5p, miR-372-3p, miR-193b-5p) miRNAs found in BG tissues (Fig. 8c). Next, we used IPA to identify target genes of the 162 BG tissue-EV miRNAs that were linked to neuroinflammation canonical pathways (Fig. 8d). The target genes were used to predict protein-protein interactions to gain insight into potential direct (physical) and indirect (functional) associations. Three gene clusters were identified (Fig. 8e). Their predicted GO biological processes detected included processes related to uterine wall breakdown, negative regulation of interleukin-23 production, positive regulation of EMT involved in endocardial cushion formation, positive regulation of tight junction disassembly, positive regulation of additional functions, and signaling pathways (Supplementary Table 7). Furthermore, we used WebGestalt to translate the 162 tissue-EV miRNA target gene lists into biological/functional insights using overrepresentation analyses (ORA) with the Benjamini-Hochberg procedure to reduce the false discovery rate and avoid type I errors. Ten functional categories were enriched, including neuron death, positive regulation of response to external stimulus, leukocyte proliferation, positive regulation of cell motility, regulation of leukocyte response to molecules of bacterial origin, T cell activation, regulation of cell-cell adhesion, positive regulation of cell activation, and extrinsic apoptotic signaling pathway (Fig. 8f). The gene list involved in each of the functional categories is presented in Supplementary Table 8.

Discussion

Despite the widespread application of multi-omics (mRNA, microRNA, and LncRNA profiling) technologies to understanding the pathogenesis of HAND, the field of "epi-transcriptomics", involving post-transcriptional regulation of gene expression via RNA modifications and editing that impacts RNA folding, stability, and interaction with its targets, remains an underexplored and understudied topic in HIV/SIV infection. Except for a few in vitro reports, there exists a dearth of knowledge about m^{6}A modifications, the most researched epi-transcriptomic modification of eukaryotic RNAs in host–HIV interactions. Moreover, the presence of m^{6}A modifications in small RNAs, such as microRNAs (miRNAs), and how HIV infection modulates m^{6}A modifications in miRNAs during infection are unknown and unexplored. We have previously described the role of miRNAs (both tissue- and extracellular vesicle-derived) in HIV/SIV-induced neuroinflammation and its modulation by long-term low-dose phytocannabinoids. Accordingly, to address this knowledge gap, we investigated the profile of BG m^{6}A methylome in host miRNAs during HIV/SIV infection and the potential effects of phytocannabinoids (THC and CBD) on the BG miRNA m^{6}A methylome. We used a combination of THC and CBD (1:3) because findings from clinical studies have confirmed that THC is well-tolerated when administered in combination with CBD[33–35]. Specifically, CBD diminished the adverse effects of THC, such as tachycardia, intoxication, and sedation, while preserving the beneficial effects of reduced muscle spasticity and neuroinflammation[33–35].

We detected m^{6}A modifications in miRNAs isolated from BG tissues of all RMs, irrespective of infection or long-term administration of low-dose phytocannabinoids (THC:CBD). Interestingly, miRNAs from BG tissues of

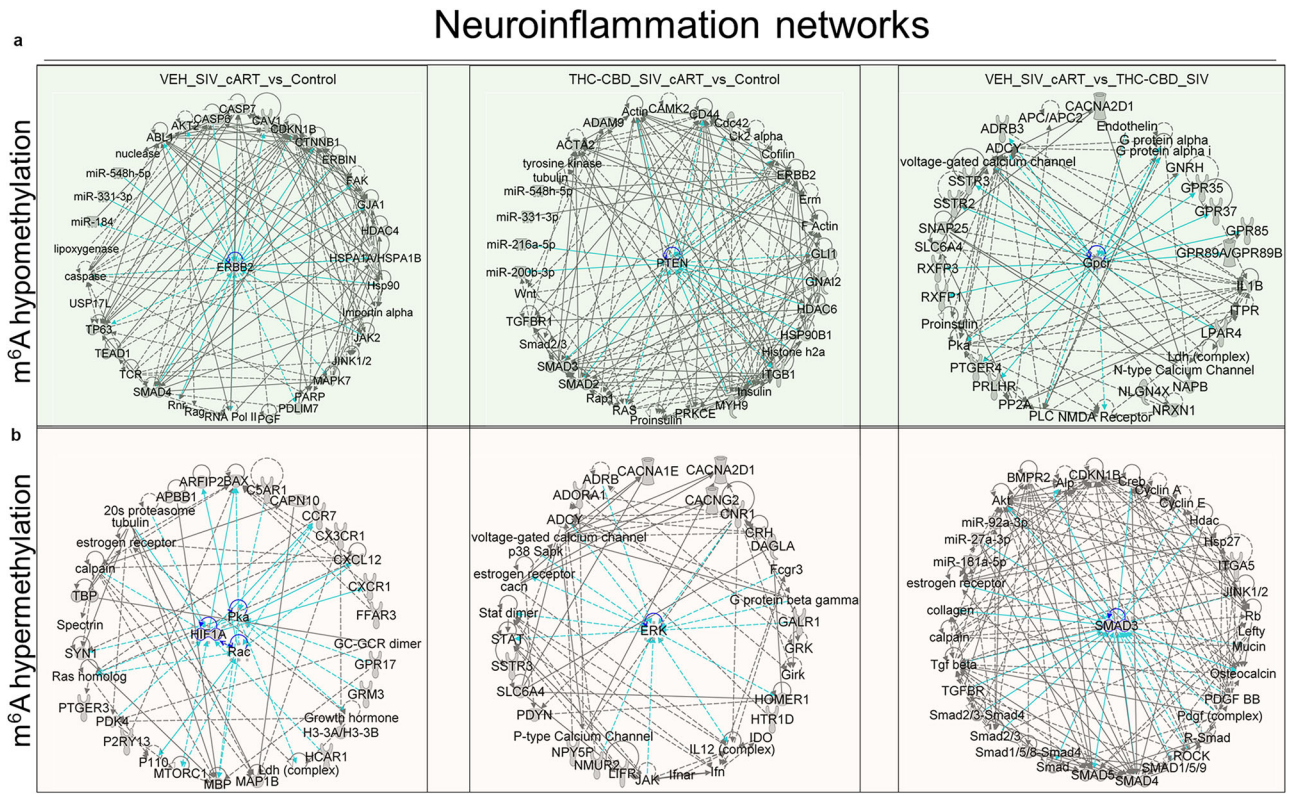

Fig. 3 | IPA Pathway analysis of m^{6}A methylation of basal ganglia derived miRNAs. a Neuroinflammation network molecules associated with the miRNAs that showed m^{6}A hypomethylation (left) or hypermethylation (right). **b** Two-way Venn diagrams of top 35 network molecules between the hypomethylated and hypermethylated miRNAs within each animal group.

VEH/SIV/ART and THC:CBD/SIV/ART RMs bore a significant hypomethylated m^{6}A profile compared to uninfected control RMs with a predictive link to neuroinflammation network genes. The potential functional impact of m^{6}A methylation on miRNA function became clearer when we performed a pathway analysis (IPA) of the genes targeted by the 44 miRNAs that were hypermethylated in BG of VEH/SIV/ART compared to THC:CBD/SIV/ART RMs (Fig. 6A). Hypermethylation of miRNA adenine nucleotides in or near the miRNA seed region (nucleotide positions 2 to 7 in the 5' seed region) can lead to loss of target mRNA 3' UTR binding and repression[36]. Therefore, in a neuroinflammatory disease like HIV/SIV infection, miRNA m^{6}A hypermethylation could lead to enhanced proinflammatory gene expression and disease progression. IPA processing of the target genes identified numerous neuroinflammatory genes such as STAT1, CCL2, CXCL12, IFNA4, TIRAP, NOS2, IL6R, and IL34, all known to promote neuroinflammation and drive progression of numerous neurological diseases such as Huntington's, Alzheimer's, and Parkinson's disease (Fig. 6B). Interestingly, others[31] and we[17] have also shown significantly increased expression of type-I IFN-stimulated genes in the brains of SIV-infected RMs. To the best of our knowledge, we provide the first evidence of the presence of m^{6}A modifications with a shift towards significant m^{6}A hypomethylation in mature miRNAs in the brain during HIV/SIV infection.

The presence of m^{6}A-modified mature miRNAs was recently reported in HEK293T[37], human lung cancer cells, and fibroblast cells in response to hypoxia[36,38]. Here, using the SIV-infected RM model, we profiled and identified differential m^{6}A methylation in both mature and PS miRNAs in whole BG tissues, although the majority of m^{6}A-modified miRNAs detected originated from the mature strand. While SIV infection and suppressive ART triggered a significant hypomethylated miRNA profile in BG tissues, miRNA expression abundance was inversely correlated to m^{6}A methylation in VEH/SIV/ART and THC:CBD/SIV/ART RMs compared to control RMs. We also identified a set of BG tissue miRNAs [(n = 162) ~ 11.1%] with m^{6}A epi-transcriptomic marks that were also present in BG EVs[18] (Fig. 8). All 162 BG tissue-EV miRNAs that bore m^{6}A marks were hypomethylated, and none were hypermethylated. Although we did not investigate the role of m^{6}A methyltransferase (writers) and demethylase (erasers) enzymes, it is important to note that the changes in m^{6}A levels on mRNAs and miRNAs are not always associated with changes in the expression levels of both enzymes. Moreover, the function of the methylation complex is multifactorial that involves posttranslational modifications such as SUMOylation of the m^{6}A-RNA methyltransferase METTL3[39], S-Adenosyl methionine (SAM, methyl donor) availability, etc., that can modulate its function. Similarly, the function of the de-methylation complex is also multifactorial, involving posttranslational modifications such as phosphorylation[40] and SUMOylation[41] at specific residues which modulates activity and ubiquitination thereby affecting protein stability and turnover. Therefore, a direct and exclusive relationship between the m^{6}A methylation levels on selected miRNAs and the activation or differentiation status of the target cells is difficult to make. Accordingly, while the activity of both enzymes is critical for the addition and removal of m^{6}A modifications, the overall levels of m^{6}A on mRNAs and miRNAs are influenced by an intricate interplay of various factors.

Next, we used IPA and WebGestalt to predict the potential functional relevance of m^{6}A-modified miRNAs. Interestingly, miRNAs bearing m^{6}A marks were found to have a link to neuroinflammation network genes, neurotransmitters/other nervous system and pathogen-influenced signaling pathways. The top three functional classifications included invasion, migration, and proliferation of cells in generalized disease states linked to the m^{6}A hypomethylation profile, while quantity of cells, organization of cytoskeleton, and neurotransmission were the important functional groups/processes found to be linked to the hypermethylated m^{6}A profile (Supplementary Table 4). PPI predicted functions and signaling pathways of BG

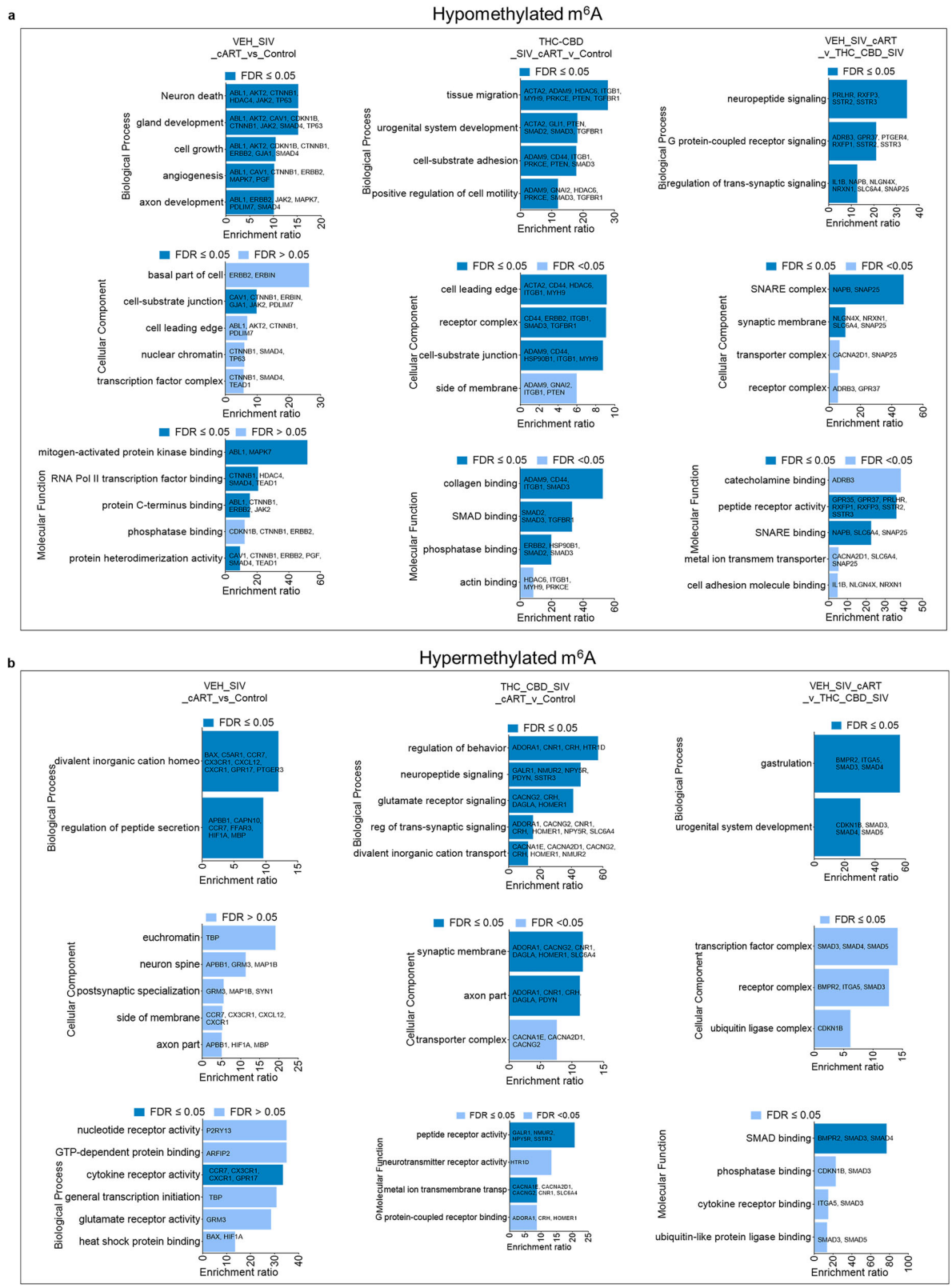

Fig. 4 | Gene ontology (GO) analysis illustrating biological processes, cellular components, and molecular functions of the neuroinflammation network molecules regulated by m^{6}A modified miRNAs. a hypomethylated and **b** hyper methylated miRNAs.

tissue m^{6}A-enriched miRNAs that were also present in BG EVs, revealing GO biological processes that included negative regulation of interleukin-23 production, positive regulation of EMT involved in endocardial cushion formation, positive regulation of tight junction disassembly, and positive regulation of calcidiol 1-monooxygenase activity (Supplementary Table 7), all with potential relevance to HIV/SIV-induced neurological disease. Recent studies have shown that m^{6}A hypermethylation in the seed regions of mature miRNAs resulted in loss of target mRNA recognition, binding, and translational inhibition[36]. Accordingly, based on these predicted functions, it is plausible that the global m^{6}A hypomethylation may be a host response to

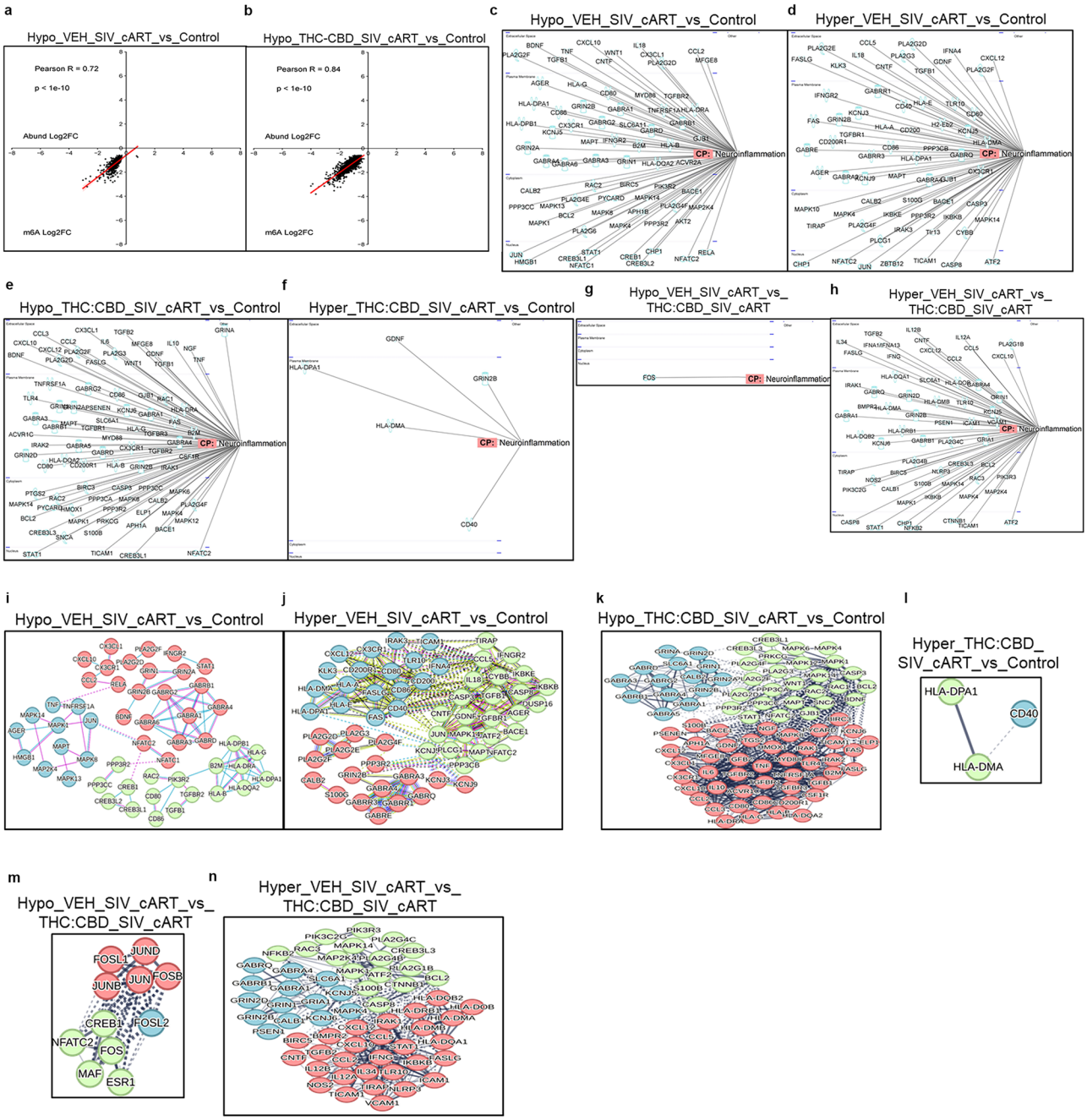

Fig. 5 | Basal ganglia miRNAs with significant m^{6}A modifications have altered expression levels. a,b Correlation analysis of m^{6}A methylation versus miRNA abundance. **c–h** Functional relationship of m^{6}A-methylated miRNAs with neurotransmitters/other nervous system and pathogen-influenced signaling pathways. **i–n** PPI networks for the IPA-identified miRNA targets in (**c–h**).

enable m^{6}A hypomethylated miRNAs to successfully regulate the expression of proinflammatory mediators, such as IL-23, STAT1, NOS1, and the blood-brain barrier integrity by promoting post-transcriptional gene silencing. Although SIV infection and ART decreased m^{6}A modifications of BG tissue miRNAs, Lichinchi et al. found that in T cells, HIV infection increased m^{6}A marks in both host and viral mRNAs[42]. Altogether, our findings show that BG miRNA m^{6}A modifications may play important roles in host–HIV interactions, as previously suggested in other viral infections, although those studies focused entirely on mRNAs[42–44] and not miRNAs.

From a functional perspective, m^{6}A miRNA modifications in BG tissues may represent a potential mechanism to regulate host miRNA-dependent regulation of proinflammatory gene expression that can directly impact HIV neuropathogenesis. This is evident from recent studies showing m^{6}A methylation of the adenine residue(s) in miR-21-5p[36], where m^{6}A modification of adenine residues near but not in the seed region resulted in loss of target gene (MAPK10 and PTEN) repression in A549 cells. Therefore, the significantly reduced m^{6}A methylation in 44 neuroinflammatory gene-targeting miRNAs in the THC:CBD/SIV/ART group compared to the VEH/SIV/ART group suggests that cannabinoids may preserve the post-transcriptional gene regulatory functions of anti-inflammatory miRNAs by reducing their m^{6}A epi-transcriptomic marks. Our recently published studies found long-term low-dose THC administration to significantly reduce type-I interferon (IFN) stimulated gene expression[17]. Since type-I IFNs activate STAT1[45], we performed bioinformatics analysis using TargetScan

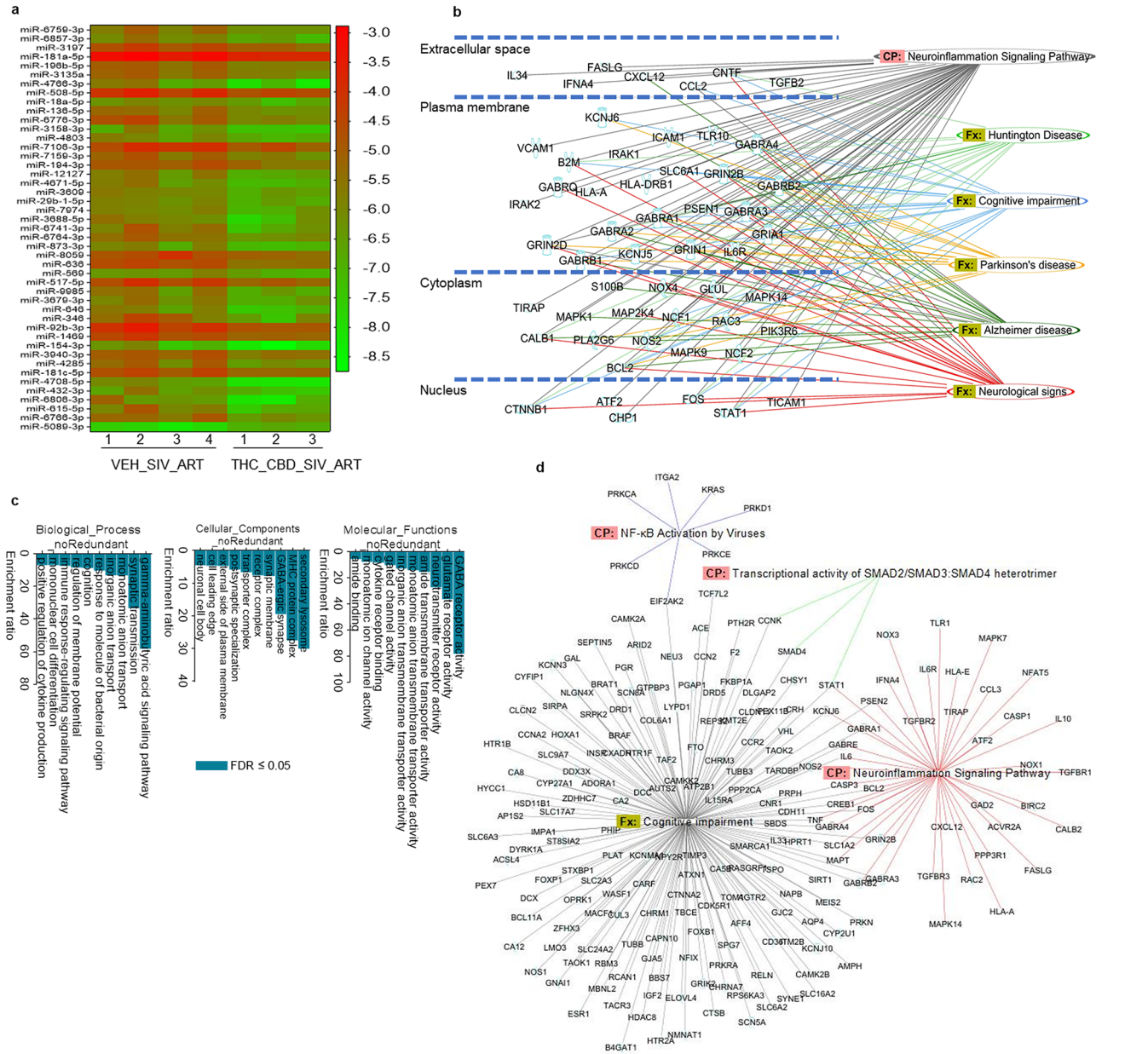

Fig. 6 | THC: CBD administration significantly reduced the incorporation of m^{6}A epitranscriptomic marks on neuroinflammation-targeting miRNAs increased by SIV infection. a Heatmap of 44 miRNAs with significant m^{6}A hypermethylation in the VEH/SIV/ART RMs relative to the THC: CBD/SIV/ART group. **b** IPA network interactome and associated canonical signaling pathways and biological functions. **c** Key biological processes, cellular components, and molecular functions regulated by 44 m^{6}A hypermethylated miRNAs. **d** IPA network of canonical signaling pathways and functions associated with 14 miRNAs with RRACH or DRACH motifs.

8.0[30] and identified RM STAT1 to be a predicted target of miR-194-5p with a perfect match between the seed sequence of miR-194-5p and the 3' UTR region of STAT1 (Fig. 7a). Interestingly, miR-194-5p showed markedly more hypomethylation in THC:CBD/SIV/ART (-1.6683 log2 fold change) than VEH/SIV/ART (-0.8617 log2 fold change) compared to control RMs. Increased STAT1 activated by IFNs is known to drive persistent neuroinflammatory signaling in a variety of neurological diseases such as Alzheimer's, Parkinson's, Huntington's disease, and traumatic brain injury. In addition, significant upregulation of IFN-stimulated STAT1 protein expression in the brain has been confirmed by others in the SIV-infected RM model[31]. We further identified a DRACH motif (where D = A, G, or U; R = A or G; and H = A, C, or U) in the seed region (nucleotides 2-7 from the 5' end) of miR-194-5p (5'- UG**UAA***C**A**GC**AACU**CCAUGUGGA-3').

Under in vitro conditions, m^{6}A methylation of adenine residues in mature miRNAs resulted in reduced suppression of target gene expression[36], suggesting that m^{6}A modification of miRNA seed nucleotides can interfere with mRNA target recognition and binding. Consistent with the findings of Wang et al.[36], in vitro overexpression of miR-194-5p mimics containing m^{6}A methylated adenosine nucleotides in the seed region failed to downregulate STAT1 protein expression, while wild-type miR-194-5p significantly reduced STAT1 protein expression at 72 h post transfection. Overall, these findings suggest that the presence of m^{6}A marks in the miR-194-5p seed region could potentially destabilize A: U pairing, thereby weakening its interactions with its binding region in the 3' UTR of STAT1 mRNA. On the contrary, reduced m^{6}A methylation of miR-194-5p can preserve its target binding capacity and represents a potential

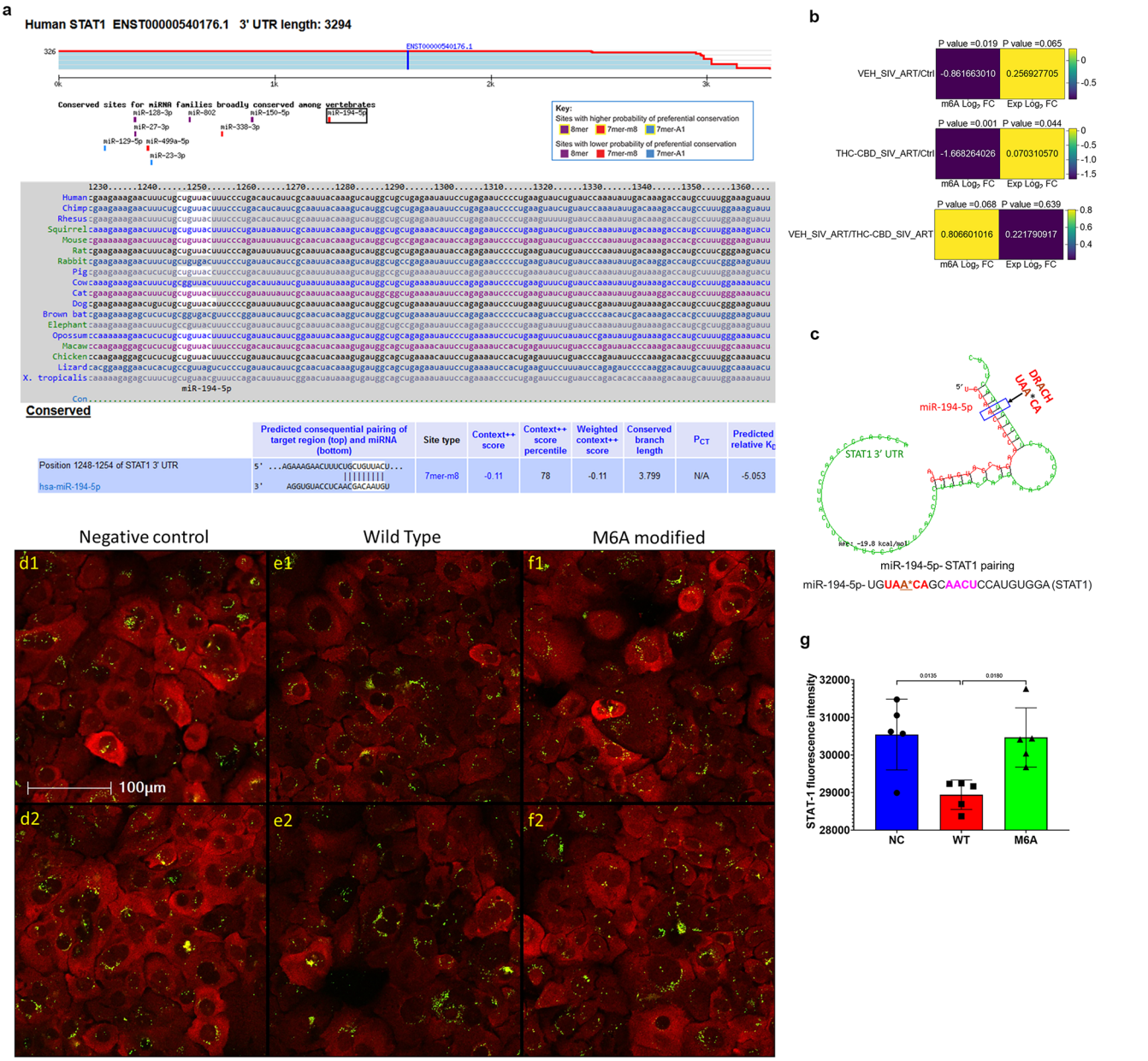

Fig. 7 | m^{6}A marks in the seed region of miR-194-5p impair its ability to post-transcriptionally silence STAT1 protein expression. a Conservation of the miR-194-5p binding site in the 3' UTR of STAT1 across twelve different mammalian species identified using TargetScan 8.0. **b** miR-194-5p fold change in VEH/SIV/ART and THC:CBD/SIV/ART relative to control rhesus macaques. **c** miR-194-5p-STAT1 pairing, as revealed by RNAhybrid, has a mean free energy change of -19.8 kcal/mole. STAT1 protein expression (red) in SCC-25 cells at 72 h post transfection with 30 nM FAM-labeled negative control mimic (**d1** and **d2**) and wild-type (**e1** and **e2**) or m^{6}A-modified (**f1** and **f2**) (green) miR-194-5p mimics and its quantification using HALO software **g**. Transfections were performed in five triplicate wells for each mimic, and experiments were repeated twice. Data were analyzed using one-way ANOVA, and post hoc analysis was done using Tukey's multiple comparisons test. A value $P < 0.05$ was considered statistically significant.

posttranscriptional gene silencing mechanism by which THC or THC:CBD may reduce STAT1 expression and accordingly reduce proinflammatory signaling in the brain and periphery. It is possible that THC: CBD may mediate these changes through altering the expression levels of m^{6}A writers and erasers that catalyze the addition and removal of m^{6}A epitranscriptomic marks. While m^{6}A marks in the miR-194-5p seed region interfered with its ability to downregulate STAT1 protein expression, it remains to be determined how m^{6}A marks in the 3' and regions adjacent to seed nucleotide impact miRNA function. Another limitation of our study is the small sample size and not addressing sex as a biological variable, since only male RMs were used in the current study. Therefore, future studies are needed to address these knowledge gaps, including whether extracellular miRNAs bear similar m^{6}A marks and the implications of such epitranscriptomic marks in HIV neuropathogenesis.

Methods

Animal care, ethics, and experimental procedures

All experiments using RMs (Table 1) were approved by the Texas Biomedical Research Institute's (Texas Biomed) Institutional Animal Care and Use Committee (IACUC Protocol# 1734MM). We have complied with all relevant ethical regulations for animal use. The Southwest National Primate Research Center (SNPRC) is an association for Assessment and Accreditation of Laboratory Animal Care International-accredited facility (AAALAC #000246). The NIH Office of Laboratory Animal Welfare assurance

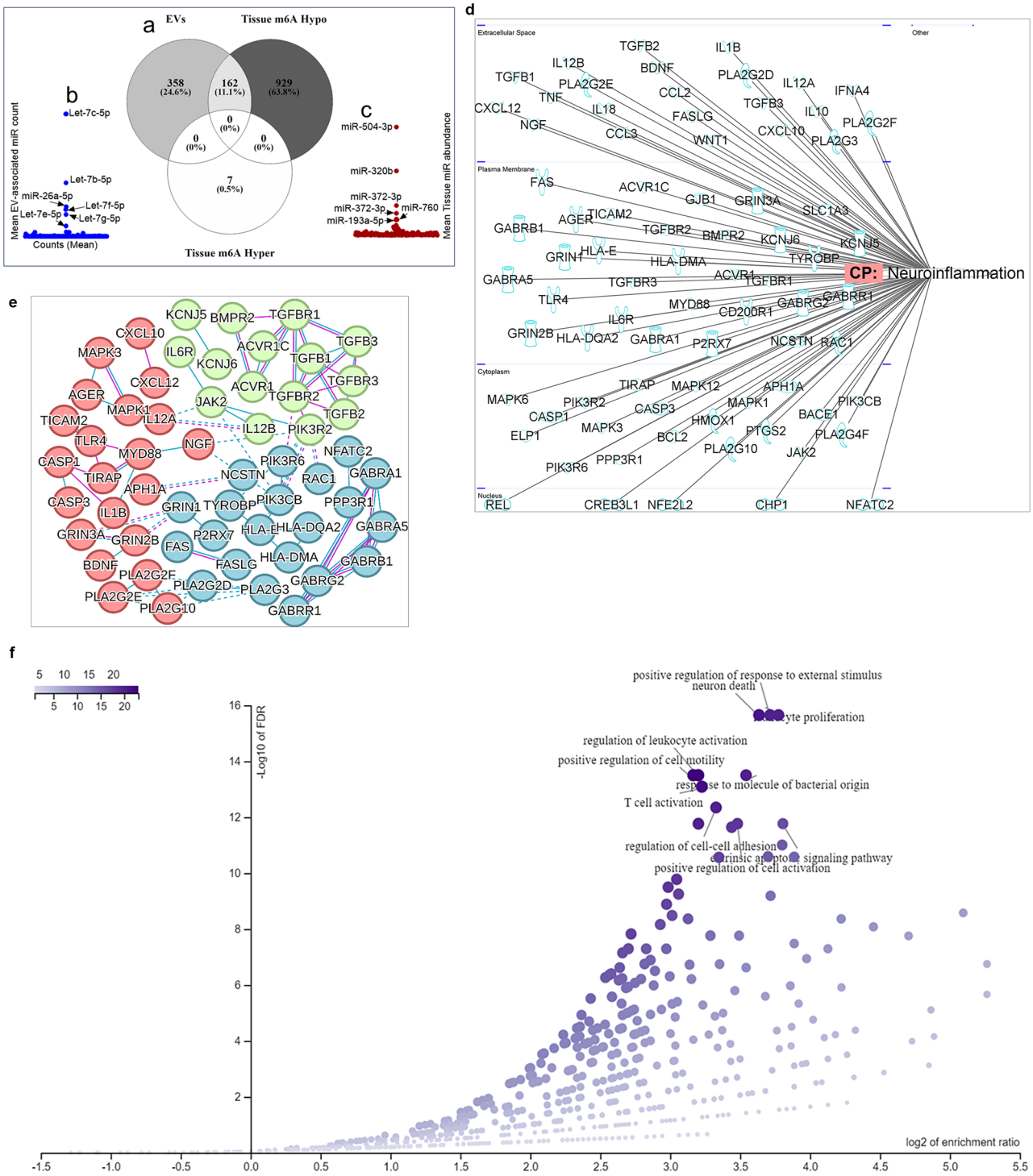

Fig. 8 | Identification of tissue-EV miRNAs with m^{6}A modification. a 3-way Venn diagram identifying m^{6}A modified tissue miRNAs present in EVs. **b** Top 5 miRNAs in EVs. C) Top 5 miRNAs in tissues. **c** Functional relationship of EV-tissue miRNAs with neurotransmitters/other nervous system and pathogen-influenced signaling pathways. **e** PPI networks for the IPA identified EV-tissue miRNA targets in panel **d**. **f** Volcano plot of biological/functional insights for EV-tissue miRNA target gene sets.

number for the SNPRC is D16-00048. All clinical procedures, including administration of anesthesia and analgesics, were carried out under the direction of a laboratory animal veterinarian. Animals were pre-anesthetized with ketamine hydrochloride, acepromazine, and glycopyrrolate, intubated, and maintained on a mixture of isoflurane and oxygen. All possible measures were taken to minimize the discomfort of all the animals used in this study. Texas Biomed complies with NIH policy on animal welfare, the Animal Welfare Act, and all other applicable federal, state, and local laws.

All RMs enrolled in this study were under the requirements of the SNPRC enrichment program. Animals were pair-housed, fed a nutritionally and fiber balanced primate diet and received daily nutritional enrichment in the form of rare or novel foods, and had continual access to toys (e.g., chew toys, N = number of animals in enclosure plus one) in the enclosure.

Additional manipulable, occupational, or sensory enrichment were available 7 days per week and changed a minimum of twice per week. These are commonly manipulable objects in the form of mirrors, bells, fidget sticks, forage devices, or other objects affixed to the enclosure (N = number of animals in enclosure).

Animal model and experimental design

Eleven age (9–10 years)- and weight (9–15 kg)-matched male Indian RMs were randomly distributed into three groups (Table 1). Group 1 [uninfected controls (n = 4)] served as uninfected controls. Groups 2-3 (n = 7) were infected intravenously with 100 times the 50% tissue culture infective dose ($100TCID_{50}$) of SIVmac251. Group 2 [VEH/SIV/ART] (n = 4) received twice-daily injections of vehicle (VEH) (1:1:18 of emulphor:ethanol:saline), intramuscularly. Group 3 [THC:CBD/SIV/ART] (n = 3) received twice-daily injections of THC:CBD (1:3 ratio) intramuscularly beginning four weeks after SIV infection at 0.18 mg/kg, as used in previous studies[17]. This dose of THC was increased to 0.32 mg/kg over a period of 2 weeks and maintained for the duration of the study. For animals in groups 2 and 3 (n = 7), ART was administered daily by subcutaneous injection and included TDF (tenofovir disoproxil fumarate) (5.1 mg/kg) (Gilead), Emtricitabine (30 mg/kg) (Gilead), and Dolutegravir (3 mg/kg) (ViiV Healthcare) and was initiated four weeks post-SIV infection (same time as initiation of THC:CBD or VEH injections). Basal ganglia (BG) tissue (~ 5 cm) was collected at necropsy from all animals. A cube of 1x1x1 cm BG tissue was used for total RNA extraction. For histopathological and immunohistochemical evaluation, BG tissues were fixed in Z-fix, embedded in paraffin, and sectioned at 5 µM thickness for histopathological analysis. SIV levels in basal ganglia were quantified using the TaqMan One-Step Real-time RT-qPCR assay that targeted the LTR gene[16]. SIV inoculum, infection duration, BG viral loads, and BG histopathology are provided in Table 1.

Methylated RNA immunoprecipitation (MeRip)

Briefly, the RNA samples were QC'd for quantity by NanoDrop ND-1000 spectrophotometer and RNA integrity by Bioanalyzer 2100 or gel electrophoresis. Briefly, 1-5 µg of each total RNA sample was immunoprecipitated using 4 µg anti-N6-methyladenosine antibody (Synaptic Systems) with 1 mg Protein G Dynabeads (Thermo Fisher, 11203D) in 500 µL RIP buffer. The modified RNAs were eluted from the immunoprecipitated magnetic beads as the "IP". The unmodified RNAs were recovered from the supernatant as "Sup". The "IP" and "Sup" RNAs were enzymatically labeled with Cy5 and Cy3, respectively in separate reactions using Arraystar's standard protocols. The labeled RNAs were combined and hybridized onto an Arraystar Human Small RNA Modification Microarray (8x15K, Arraystar), and the array was scanned in two-color channels by an Agilent Scanner G2505C. Agilent Feature Extraction software (version 11.0.1.1) was used to analyze the acquired array images. Raw intensities of IP (immunoprecipitated, Cy5-labeled) and Sup (supernatant, Cy3-labeled) were normalized with the average of log2-scaled spike-in RNA intensities. After normalization, the probe signals having Present (P) or Marginal (M) QC flags in at least 4 out of 12 samples were retained. Multiple probes from the same small RNA (miRNA/TsRNA (tRF&tiRNA)/pre-miRNA) sample were combined into one RNA level. "m^6A abundance" was analyzed based on the Cy5-labelled IP (modified RNA) normalized intensities. Differentially m^6A-modified RNAs between two comparison groups were identified by fold change (FC) and statistical significance (p-value) thresholds. A hierarchical Clustering heatmap was plotted to display m^6A-modification patterns among samples by R software.

RNA processing and m^6A analyses

Basal ganglia tissues were collected during necropsy in 1 cm^3 cubes and processed for total RNA extraction using Qiazol (Qiagen Inc., CA). Briefly, total RNA was immunoprecipitated with anti-N6-methyladenosine (m^6A) antibody, and the modified RNAs were eluted from the beads as " m^6A", and unmodified RNAs were recovered as "unmodified" samples. Raw intensities of each sample were normalized with the average of log2-scaled spike-in RNA intensities. Differentially m^6A-modified RNAs between two comparison groups were identified by fold change (FC) and statistical significance (p-value) thresholds. A hierarchical Clustering heatmap was plotted to display m^6A modification patterns among samples by R software.

Criteria for selecting m^6A modified miRNA

Differentially significant m^6A methylated miRNAs were identified with p-value < 0.05, | log2(FC)| > 1 upregulation, and <-1 downregulation. To identify m^6A-modified miRNAs that are biologically relevant to HIV/SIV-induced neuroinflammation, we used the miRNA Target Filter functionality of IPA with a set of criteria to prioritize experimentally validated and predicted mRNA targets to perform enrichment analysis. Based on confidence level, diseases, cells/tissues, and pathways, we identified miRNA-mRNA interactions, overlaid miRNA data onto network pathways, and molecules. The identified miRNA target genes were fed into the WEB-based GEne SeT AnaLysis Toolkit (WebGestalt, https://www.webgestalt.org/) and used for Gene Ontology analysis. The following criteria were used:

Tissue = Brain

Pathway = Neurotransmitters and other nervous system signaling

Disease = neurological diseases

Network overlay = neuroinflammation canonical signaling pathway. Merge multiple relevant networks.

Used IPA-generated list for STRING: functional protein association networks (https://string-db.org/) for protein-protein analysis.

Used IPA-generated list for WEB-based Gene SeT AnaLysis Toolkit (WebGestalt) GO biological, cellular, and molecular processes analyses, using overrepresentation analysis (ORA) enrichment method.

Cell culture and in vitro transfection studies

We determined the impact of miR-194-5p m^6A on STAT1 using the human squamous cell carcinoma (SCC-25) epithelial-like cell line (ATCC.org CAT# CRL-1628), as this cell line expressed high basal levels of STAT1 protein. SCC-25 cells were cultured in a 1:1 mixture of DMEM and F12 medium (Thermo Fisher Scientific, Waltham, MA, USA) containing 1.2 g/L sodium bicarbonate, 2.5 mM L-glutamine, 15 mM HEPES, and 0.5 mM sodium pyruvate and supplemented with 10% FBS in 8-well chamber slides (Cellvis, Mountain View, CA, USA) at 37 °C in a humidified atmosphere with 5% CO_2. At 90% confluency, cells were transfected with 30 nM of negative control, miR-194-5p-Wild type or miR-194-5p-m^6A mimic using the Lipojet transfection reagent (Signagen, DE). Each treatment was performed in five replicates and repeated twice. At 72 h post-transfection, cells were fixed with 2% paraformaldehyde and immunostained with STAT1 and later with DAPI for nuclear localization.

Immunofluorescence staining, confocal microscopy and data analysis

Immunofluorescence staining for the detection of STAT1 in SCC-25 cells transfected with negative control, wild-type miR-194-5p, and m^6A-modified miR-194-5p mimics was performed using a STAT1 monoclonal antibody (Cell Signaling Technology; Cat# 14994 T) (1:200 dilution). A total of 5 images were taken from each well using a Zeiss LSM700 confocal microscope (Carl Zeiss Microscopy, LLC) at 20X objective. Digital images were imported into HALO software (Indica Labs) for image quantitation analysis. Area quantification module FL v2.3.4 on HALO v3.6 (Indica Labs) was used to quantify STAT1 fluorescence intensity (red signal/Alexa-568). Artificial intelligence-driven HALO software identifies all cells that express STAT1 in red and nuclei in blue (DAPI) and categorizes the cells based on fluorescence intensity levels. The average fluorescence intensity per transfected well (5 replicates per condition) in 8-well chambers was calculated, and the data were graphed using Prism v9 (GraphPad Prism software).

Statistical and reproducibility

Agilent Feature Extraction software (version 11.0.1.1) was used to analyze the acquired array images. Raw intensities of IP (immunoprecipitated,

Cy5-labelled) and Sup (supernatant, Cy3-labelled) were normalized with average of log2-scaled Spike-in RNA intensities. After normalization, the probe signals having Present (P) or Marginal (M) QC flags in at least 4 out of 11 samples were retained. Multiple probes from the same small RNA (miRNA/tsRNA/pre-miRNA) were combined into one RNA level. "m^6A abundance" was analyzed based on the Cy5-labelled IP (modified RNA) normalized intensities. Differentially m^6A-methylated RNAs between two comparison groups were identified by fold change (FC) and statistical significance (p-value) thresholds. Hierarchical Clustering heatmap was plotted to display m^6A-modification patterns among samples by R software.

Pie charts were generated using GraphPad Prism. Heatmaps were generated with GraphPad Prism and Heatmapper (http://heatmapper.ca/). Venn diagrams were generated with Venny 2.1 (https://bioinfogp.cnb.csic.es/tools/venny/). miR-194-5p transfection experiments were performed in five triplicate wells for each of three mimics, and experiments were repeated twice. Changes in STAT1 protein expression in response to miR-194-5p transfection were analyzed using one-way ANOVA. Post hoc analysis was performed using Tukey's multiple comparisons test. The Shapiro-Wilk test (GraphPad Prism) was used to test data normality.

Reporting summary

Further information on research design is available in the Nature Portfolio Reporting Summary linked to this article.

Data availability

MicroRNA m^6A methylation raw data has been submitted to GEO with ID GSE296015 and can be accessed using the link (https://www.ncbi.nlm.nih.gov/geo/query/acc.cgi?acc=GSE296015). The numerical source data for all graphs in the manuscript can be found in the excel file named Supplementary Data 1.

Received: 19 December 2024; Accepted: 14 October 2025;
Published online: 24 November 2025

References

1. Eden, A. et al. HIV-1 viral escape in cerebrospinal fluid of subjects on suppressive antiretroviral treatment. *J. Infect. Dis.* **202**, 1819–1825 (2010).
2. Lamers, S. L., Gray, R. R., Salemi, M., Huysentruyt, L. C. & McGrath, M. S. HIV-1 phylogenetic analysis shows HIV-1 transits through the meninges to brain and peripheral tissues. *Infect. Genet Evol.* **11**, 31–37 (2011).
3. Spudich, S., Lollo, N., Liegler, T., Deeks, S. G. & Price, R. W. Treatment benefit on cerebrospinal fluid HIV-1 levels in the setting of systemic virological suppression and failure. *J. Infect. Dis.* **194**, 1686–1696 (2006).
4. Grant, I. et al. Evidence for early central nervous system involvement in the acquired immunodeficiency syndrome (AIDS) and other human immunodeficiency virus (HIV) infections. Studies with neuropsychologic testing and magnetic resonance imaging. *Ann. Intern Med.* **107**, 828–836 (1987).
5. Sacktor, N. et al. Prevalence of HIV-associated neurocognitive disorders in the Multicenter AIDS cohort study. *Neurology* **86**, 334–340 (2016).
6. Fuster-RuizdeApodaca, M. J. et al. Prevalence and patterns of illicit drug use in people living with HIV in Spain: a cross-sectional study. *PloS ONE* **14**, e0211252 (2019).
7. Castro, F. O. F. et al. Distinct inflammatory profiles in HIV-infected individuals under antiretroviral therapy using cannabis, cocaine or cannabis plus cocaine. *AIDS* **33**, 1831–1842 (2019).
8. Galaj, E., Bi, G. H., Yang, H. J. & Xi, Z. X. Cannabidiol attenuates the rewarding effects of cocaine in rats by CB2, 5-HT(1A) and TRPV1 receptor mechanisms. *Neuropharmacology* **167**, 107740 (2020).
9. Mimiaga, M. J. et al. Substance use among HIV-infected patients engaged in primary care in the United States: findings from the Centers for AIDS Research Network of Integrated Clinical Systems cohort. *Am. J. public health* **103**, 1457–1467 (2013).
10. Mohammadi, A. et al. Effect of opium addiction on lipid profile and atherosclerosis formation in hypercholesterolemic rabbits. *Exp. Toxicol. Pathol. Off. J. Ges. fur Toxikologische Pathologie* **61**, 145–149 (2009).
11. Roohafza, H. et al. Opium decreases the age at myocardial infarction and sudden cardiac death: a long- and short-term outcome evaluation. *Arch. Iran. Med.* **16**, 154–160 (2013).
12. Nabati, S. et al. The plasma levels of the cytokines in opium-addicts and the effects of opium on the cytokines secretion by their lymphocytes. *Immunol. Lett.* **152**, 42–46 (2013).
13. Saha, B., Momen-Heravi, F., Kodys, K. & Szabo, G. MicroRNA cargo of extracellular vesicles from alcohol-exposed monocytes signals naive monocytes to differentiate into M2 macrophages. *J. Biol. Chem.* **291**, 149–159 (2016).
14. Momen-Heravi, F. et al. Increased number of circulating exosomes and their microRNA cargos are potential novel biomarkers in alcoholic hepatitis. *J. Transl. Med.* **13**, 261 (2015).
15. Momen-Heravi, F., Bala, S., Kodys, K. & Szabo, G. Exosomes derived from alcohol-treated hepatocytes horizontally transfer liver specific miRNA-122 and sensitize monocytes to LPS. *Sci. Rep.* **5**, 9991 (2015).
16. McDew-White, M., et al. Cannabinoid control of gingival immune activation in chronically SIV-infected rhesus macaques involves modulation of the indoleamine-2,3-dioxygenase-1 pathway and salivary microbiome. *EBioMedicine* **75**, 103769 (2022).
17. McDew-White, M., et al. Cannabinoids modulate the microbiota-gut-brain axis in HIV/SIV infection by reducing neuroinflammation and dysbiosis while concurrently elevating endocannabinoid and indole-3-propionate levels. *J. Neuroinflammation* **20**, 62 (2023).
18. Kaddour, H. et al. Chronic delta-9-tetrahydrocannabinol (THC) treatment counteracts SIV-induced modulation of proinflammatory microRNA cargo in basal ganglia-derived extracellular vesicles. *J. Neuroinflammation* **19**, 225 (2022).
19. Jonkhout, N. et al. The RNA modification landscape in human disease. *RNA* **23**, 1754–1769 (2017).
20. Fan, Y., Lv, X., Chen, Z., Peng, Y. & Zhang, M. m6A methylation: critical roles in aging and neurological diseases. *Front. Mol. Neurosci.* **16**, 1102147 (2023).
21. Zhang, F. et al. Regulation of N6-methyladenosine (m6A) RNA methylation in microglia-mediated inflammation and ischemic stroke. *Front. Cell Neurosci.* **16**, 955222 (2022).
22. Chatterjee, B., Shen, C. J. & Majumder, P. RNA modifications and RNA metabolism in neurological disease pathogenesis. *Int. J. Mol. Sci.* **22**, 11870 (2021).
23. Hill, M. & Tran, N. Global miRNA to miRNA Interactions: impacts for miR-21. *Trends Cell Biol.* **31**, 3–5 (2021).
24. Ooi, J. Y. Y. et al. Identification of miR-34 regulatory networks in settings of disease and antimiR-therapy: Implications for treating cardiac pathology and other diseases. *RNA Biol.* **14**, 500–513 (2017).
25. Wang, D. et al. Nuclear miR-122 directly regulates the biogenesis of cell survival oncomiR miR-21 at the posttranscriptional level. *Nucleic Acids Res.* **46**, 2012–2029 (2018).
26. Price, A. M. et al. Direct RNA sequencing reveals m(6)A modifications on adenovirus RNA are necessary for efficient splicing. *Nat. Commun.* **11**, 6016 (2020).
27. Kashima, R. & Hata, A. The role of TGF-beta superfamily signaling in neurological disorders. *Acta Biochim Biophys. Sin.* **50**, 106–120 (2018).
28. Su, C., Miao, J. & Guo, J. The relationship between TGF-beta1 and cognitive function in the brain. *Brain Res. Bull.* **205**, 110820 (2023).
29. Deng, Z. et al. TGF-beta signaling in health, disease, and therapeutics. *Signal Transduct. Target Ther.* **9**, 61 (2024).
30. Agarwal, V., Bell, G. W., Nam, J. W. & Bartel, D. P. Predicting effective microRNA target sites in mammalian mRNAs. *Elife* **4**, 5005 (2015).

31. Roberts, E. S. et al. Acute SIV infection of the brain leads to upregulation of IL6 and interferon-regulated genes: expression patterns throughout disease progression and impact on neuroAIDS. *J. Neuroimmunol.* **157**, 81–92 (2004).
32. Rehmsmeier, M., Steffen, P., Hochsmann, M. & Giegerich, R. Fast and effective prediction of microRNA/target duplexes. *Rna* **10**, 1507–1517 (2004).
33. Cooper, D. B. et al. Treatment of persistent post-concussive symptoms after mild traumatic brain injury: a systematic review of cognitive rehabilitation and behavioral health interventions in military service members and veterans. *Brain Imaging Behav.* **9**, 403–420 (2015).
34. Russo, E. & Guy, G. W. A tale of two cannabinoids: the therapeutic rationale for combining tetrahydrocannabinol and cannabidiol. *Med Hypotheses* **66**, 234–246 (2006).
35. Vermersch, P. Sativex(®) (tetrahydrocannabinol + cannabidiol), an endocannabinoid system modulator: basic features and main clinical data. *Expert Rev. Neurother.* **11**, 15–19 (2011).
36. Wang, H., Song, X., Song, C., Wang, X. & Cao, H. m(6)A-seq analysis of microRNAs reveals that the N6-methyladenosine modification of miR-21-5p affects its target expression. *Arch. Biochem Biophys.* **711**, 109023 (2021).
37. Berulava, T., Rahmann, S., Rademacher, K., Klein-Hitpass, L. & Horsthemke, B. N6-adenosine methylation in MiRNAs. *PloS one* **10**, e0118438 (2015).
38. van den Homberg, D. A. L., van der Kwast, R., Quax, P. H. A. & Nossent, A. Y. N-6-Methyladenosine in Vasoactive microRNAs during Hypoxia; A Novel Role for METTL4. *Int. J. Mol. Sci.* **23**, 1057 (2022).
39. Du, Y. et al. SUMOylation of the m6A-RNA methyltransferase METTL3 modulates its function. *Nucleic Acids Res.* **46**, 5195–5208 (2018).
40. Cao, L. et al. A LATS2 and ALKBH5 positive feedback loop supports their oncogenic roles. *Cell Rep.* **43**, 114032 (2024).
41. Yu, F. et al. Post-translational modification of RNA m6A demethylase ALKBH5 regulates ROS-induced DNA damage response. *Nucleic Acids Res.* **49**, 5779–5797 (2021).
42. Lichinchi, G., et al. Dynamics of the human and viral m(6)A RNA methylomes during HIV-1 infection of T cells. *Nat. Microbiol.* **1**, 16011 (2016).
43. Lichinchi, G. & Rana, T. M. Profiling of N(6)-Methyladenosine in Zika Virus RNA and Host Cellular mRNA. *Methods Mol. Biol.* **1870**, 209–218 (2019).
44. Lichinchi, G. et al. Dynamics of human and Viral RNA methylation during Zika virus infection. *Cell Host Microbe* **20**, 666–673 (2016).
45. Platanias, L. C. Mechanisms of type-I- and type-II-interferon-mediated signalling. *Nat. Rev. Immunol.* **5**, 375–386 (2005).

Acknowledgements

The authors would like to thank the veterinary staff and pathology personnel at the Southwest National Primate Research Center for their assistance in animal work and necropsy sample collection. This work was supported by National Institutes of Health funding (Grant No. R01DA042348 [to CMO]; Grant No. R01DA052845 [to MM], Grant Nos. R01DA050169 and R21/R33DA053643 [to CMO & MM], Grant No. R33MH112360 [to CST], R01CA218500, UH3TR002881, R01TR218500 [to IG], P30AI161943, and P51OD111033. Research reported in this publication was supported by the Office of the Director, National Institutes of Health under Award Numbers S10OD028732 and S10OD032443. The content is solely the responsibility of the authors and does not necessarily represent the official views of the National Institutes of Health.

Author contributions

Study conceptualization and design: I.G., C.S.T., and M.M. C.M.O. conducted data analyses. C.M.O., M.M., and I.G. wrote the original draft, reviewed and edited the manuscript. I.G., L.S.P., and M.M. performed the in vitro m^6A miR-194-5p overexpression and immunofluorescence studies and HALO image analysis and quantification. L.S.P. assisted with manuscript proof reading and preparation of animal information.

Competing interests

The authors declare no competing interests.

Additional information

Supplementary information The online version contains supplementary material available at https://doi.org/10.1038/s42003-025-09049-w.

Correspondence and requests for materials should be addressed to Chioma M. Okeoma, Ionita C. Ghiran or Mahesh Mohan.

Peer review information *Communications Biology* thanks the anonymous reviewers for their contribution to the peer review of this work. Primary Handling Editors: Joao Valente. A peer review file is available.